



SRTTU

Journal of Computational and Applied Research  
in Mechanical Engineering

jcarme.sru.ac.ir

JCARME

ISSN: 2228-7922

## Research paper

## Numerical study of built-in cylinders' effects on flow pattern and heat transfer characteristics in a laminar channel flow

Sajad Rezazadeh<sup>a,\*</sup>, Mohammadreza Mataji Amirrud<sup>b</sup>, Mohammad Raad<sup>a</sup> and Davoud Abbasinezhad Fallah<sup>a</sup>

<sup>a</sup>Faculty of Mechanical Engineering, Urmia University of Technology, Urmia, Iran.

<sup>b</sup>Faculty of Energy and Environment Department, School of Environment, College of Engineering, University of Tehran, Tehran, Iran.

### Article info:

#### Article history:

Received: 06/05/2020  
Revised: 20/12/2020  
Accepted: 23/12/2020  
Online: 27/12/2020

#### Keywords:

Reynolds number,  
Blockage ratio,  
Strouhal number,  
Nusselt number,  
Performance index.

#### \*Corresponding author:

[sor.mems@gmail.com](mailto:sor.mems@gmail.com)

### Abstract

A numerical simulation of laminar fluid flow and heat transfer over built-in cylinders in a channel is presented. Effects of cylinders that located in a rectangular channel with constant wall temperature on flow and heat transfer have been investigated by the drag coefficient on cylinders wall, skin-friction factor on channel wall, Strouhal number, pumping factor, Nusselt number, and Performance Index (PI) factor, which denote the heat transfer in terms of the pressure drop. Results are validated by the most reliable published works in the literature. Effects of Reynolds number and blockage ratio ( $\beta$ ) for the equilateral triangular cylinder for  $120 \leq Re \leq 180$  and  $0.15 \leq \beta \leq 0.55$  on flow and heat transfer are investigated with more details. Results indicated that by increasing Re for constant blockage ratio, the drag coefficient, Strouhal number, and Nusselt number increase; but the skin-friction coefficient, pumping factor, and PI factor decrease subsequently. Additionally, with an increase in blockage ratio at constant Re, the drag coefficient, skin-friction coefficient, pumping factor, and Strouhal number grow up; but Nusselt number diminishes and PI factor has an optimum range. Furthermore, results reveal that variation in blockage ratio has more significant effects on the flow and heat transfer than variation in Reynolds number.

## 1. Introduction

The classical problem of flow over bluff bodies is a major interest in the fluid mechanics, due to its relevancy to engineering applications, e.g. suspension of bridges, automobile manufacturing, aerospace, chemical engineering, cooling of

the electronic components, etc. [1-6]. Also, more recently, with increasing demand in energy consumption, this problem gains additional interest in the field of magnetohydrodynamic electricity production [7-9]. Pertinently, this problem has been one of the major topics for investigation by numerous scientists [10]. In 1969, Johnson and Joubert [11] experimentally studied the effects

of vortex generators (VG) on airstream by using a cylinder which was fitted with two rows of VGs. Their results show both a decrease in drag coefficient and an increase in Nusselt number that can be obtained when VGs are fitted. Noack and Eckelmann [12] practiced Galerkin method to investigate flow over a circular cylinder. They obtained the beginning of the laminar vortex shedding at  $Re_{crit}=53.3$  and this regime lasts until  $Re=170$  which induces three-dimensional calculations due to 3-D instabilities of flow. Zdravkovich [13] presented a classification of flow over circular cylinder and ascribed periodic laminar wake to  $30-40 < Re < 150-200$ . Williamson [14] conducted a comprehensive classification of this problem by means of the base suction coefficient and showed that the laminar vortex shedding regime happens at  $49 < Re < 140-194$ . Suzuki et al. [15] investigated the numerical solution for unsteady laminar flow over a square rod placed at the channel center. They considered variation of the blockage ratio and Reynolds number, and they found that the blockage ratio is a major factor in appearance of the periodic motion of the flow. The numerical investigation of flow and heat transfer characteristics of a heated square cylinder in laminar channel flow was carried out by Sharma and Eswaran [16]. They observed increase in Strouhal number, drag coefficient, pumping power, and cylinder's Nusselt number in proportion to increase in blockage ratio. Additionally, in their earlier publication [17], they found that onset of unsteady periodicity occurs for  $Re \geq 50$ . Also, Tatsutani et al. [18] studied this problem for a tandem of heated square cylinder; and Valencia [19] conducted a numerical study on flow and heat transfer in channel with a tandem of rectangular cylinder for a range of the Reynolds number between 100 and 400 and four different cylinder separation distances. Findings showed that the flow oscillations occur at  $Re > 100$  when the Reynolds number is based on the channel height; and the heat transfer from side walls of the channel increases by a factor of 1.78 in comparison with the plane channel. In 2007, De and Dalal [20] carried out a study on a heated triangular cylinder in laminar channel flow for a range of the Reynolds number based on maximum inlet velocity between 80 and 200 and a range of blockage ratio between 1/12 and

1/3. Their results showed that the Strouhal number and RMS of lift coefficient increase significantly with blockage ratio and Reynolds number while overall Nusselt number on triangular cylinder remains almost unchanged for different blockage ratios. Srikanth et al. [21] studied this problem for a range of Reynolds numbers between 1 and 80 and fixed blockage ratio of 0.25. They observed that the average Nusselt number and wake length increase and the mean drag coefficient decrease with increasing the Reynolds number. Also, they found critical Reynolds numbers between 58 and 59. Moreover, Ali et al. [22] experimentally investigated this problem for two positions of the equilateral triangular cylinder, when the vertex of the triangle faces the flow and the flat surface faces the flow, for a range of blockage ratios and a wide range of Reynolds numbers for turbulent regime. Effects of proximity of the channel wall to the triangular cylinder on flow and heat transfer from the channel side for Reynolds number ranges of 100–450 was numerically investigated by Farhadi et al. [23]. Results revealed that as triangular cylinder approaches the wall, the vortex shedding is removed and subsequently the heat transfer rate decreases. Yoon et al. [10] parametrically investigated the flow over inclined square cylinders to analyze different shedding topologies exhibited by the flow and also critical Reynolds numbers as the cylinder inclination varies from a symmetric to an asymmetric alignment about the horizontal centerline. Also, Agrwal et al. [24] experimentally studied the wake characteristics of a cylinder at several various inclinations at  $Re=520$ . Bao et al. [25] numerically investigated the flow past an equilateral cylinder using a two-step Taylor characteristic-based Galerkin method at different angles ( $\alpha$ ) of flow. Results revealed that the triangular cylinder at  $\alpha=0$  (side facing flow) experiences a higher drag force than the cylinder at  $\alpha=60$  (apex facing flow). Tu et al. [26] studied the flow induced forces and flow characteristics of a triangular cylinder with various incident angles (0–60) at a wide range of Reynolds numbers ( $Re=50-160$ ). It is seen that the incident angle greatly alters pressure distribution around the triangular cylinder. Several studies on flows over the cylinder have been carried out to analyze the thermal behavior of the

flow [27,28]. Chatterjee and Mondal [29] numerically analyzed unsteady flow and heat transfer case over a bluff body for different values of Prandtl number ( $Pr = 0.71, 7$  and  $100$ ). Their results showed that the increase in Reynolds number affects the distribution of isotherms behind the body which results in reducing the heat transfer.

From flow field characteristics view point, generally, flow around bluff bodies is influenced by three distinct regions: boundary layer (continues from stagnation point to the separation point), shear-layer (from separation point to the closure of the recirculation bubble), and wake (from end of recirculation zone to the downstream where it refers to the shear-layers merge). Features of these regions at different Reynolds numbers is the basis of categorizing flow into six regimes: no separation (creeping flow), a fixed pair of symmetric vortices, laminar vortex street, transition to turbulence in the wake, wake completely turbulent but laminar boundary layer, and turbulent wake and boundary layer. This paper is allocated to investigate the flow around bluff bodies in laminar boundary layer and wake where the most variation in flow characteristics (e.g. Strouhal number) happens.

Although several investigations set out to study the effects of bluff bodies on flow and heat transfer, various aspects of this problem have been remained unknown. This paper aims to investigate the effects of a triangular cylinder and six other different shapes of cylinders on heat transfer from side walls of the rectangular channel. It examines the drag coefficient on cylinder sides, skin-friction coefficient and Nusselt number on the channel wall, pumping factor, and Strouhal number for each model. Finally, efficiency of each cylinder shape in the enhancement of heat transfer is analyzed by the PI factor.

## 2. Numerical simulation

### 2.1. Assumptions

All models are simulated by commercial software COMSOL Multiphysics 5.2a under the assumptions of laminar, incompressible, and unsteady flow. Also, the flow is assumed to be two-dimensional to prevent extra computational cost. The working fluid, air ( $Pr=0.71$ ), is assumed to

be Newtonian, and the viscous dissipation is neglected. Maximum temperature difference between the inlet fluid and the wall of the channel is  $2K$ , so the physical properties are assumed to be constant.

### 2.2. Governing equations

As aforementioned assumptions are applied, the dimensionless mass conservation, x and y components of momentum, and energy conservation equations are transformed as follows respectively.

$$\frac{\partial u}{\partial x} + \frac{\partial v}{\partial y} = 0 \quad (1)$$

$$\frac{\partial u}{\partial t} + u \frac{\partial u}{\partial x} + v \frac{\partial u}{\partial y} = -\frac{\partial P}{\partial x} + \frac{1}{Re} \left( \frac{\partial^2 u}{\partial x^2} + \frac{\partial^2 u}{\partial y^2} \right) \quad (2)$$

$$\frac{\partial v}{\partial t} + u \frac{\partial v}{\partial x} + v \frac{\partial v}{\partial y} = -\frac{\partial P}{\partial y} + \frac{1}{Re} \left( \frac{\partial^2 v}{\partial x^2} + \frac{\partial^2 v}{\partial y^2} \right) \quad (3)$$

$$\frac{\partial \theta}{\partial t} + u \frac{\partial \theta}{\partial x} + v \frac{\partial \theta}{\partial y} = \frac{1}{Re \cdot Pr} \left( \frac{\partial^2 \theta}{\partial x^2} + \frac{\partial^2 \theta}{\partial y^2} \right) \quad (4)$$

$u, v, x, y, t, \theta, P, Re,$  and  $Pr$  are dimensionless x and y components of velocity, axial and transverse coordinates (Cartesian), time, temperature, pressure, Reynolds number, and Prandtl number are defined respectively as follows:

$$u = \frac{u^*}{U_{in}}, \quad v = \frac{v^*}{U_{in}}, \quad x = \frac{x^*}{H}, \quad y = \frac{y^*}{H},$$

$$t = \frac{t^* U_{in}}{L}, \quad \theta = \frac{T - T_{in}}{T_w - T_{in}}, \quad P = \frac{P^*}{\rho U_{in}^2},$$

$$Re = \frac{\rho U_{in} b}{\mu}, \quad Pr = \frac{\mu C_p}{k}$$

where superscript \* is related to dimensional variables, and subscripts  $in$  and  $w$  denote inlet and wall conditions.  $U_{in}, H, L, T, \rho, \mu, C_p,$  and  $k$  are, respectively, the maximum of inlet velocity, channel height, channel length ( $L=10H$ ), dimensional temperature, density, dynamic viscosity, specific heat at constant pressure, and thermal conductivity.

### 2.3. Boundary conditions

Inlet conditions are given as follows:

$$\begin{cases} u = 1 - \left( \left| 1 - \frac{2y}{H} \right| \right)^2 \\ v = 0 \end{cases} \quad (5)$$

and  $\theta = 0$ . In COMSOL Multiphysics 5.2a; it is recommended to use a step function for ramping up the inlet velocity due to avoiding inconsistency between initial and inlet conditions.

Velocity conditions on walls are defined as no-slip ( $u = 0$  and  $v = 0$ ) and thermal conditions on channel walls are  $\partial\theta/\partial y = 0$  for  $x < x_s$  and  $x > x_e$ ,  $\theta = 1$  for  $x_s \leq x \leq x_e$ , and on cylinder surface is  $\partial\theta/\partial n = 0$  where  $n$  is the normal direction to cylinder surface.

Outlet conditions are  $P = 0$ , which is defined relative to atmosphere pressure, and  $\partial\theta/\partial x = 0$ .

#### 2.4. Defined numbers

Efficiency of channel in enhancement of heat transfer with regard to pressure drop is denoted by Eq. (6).

$$PI = \frac{\overline{Nu} / \overline{Nu}_0}{\left( f / f_0 \right)^{1/3}} \quad (6)$$

where  $Nu$  and  $f$  that are the Nusselt number and pumping factor, are presented in Eqs. (7 and 8).

$$Nu = \frac{\sqrt{\left( \frac{\partial T}{\partial x} \right)^2 + \left( \frac{\partial T}{\partial y} \right)^2} \times H}{T_w - T_{in}} \quad (7)$$

$$f = \frac{2D_H \Delta P}{L} \quad (8)$$

where  $\Delta P$  is the non-dimensional pressure difference between inlet and outlet and  $D_H$  is the hydraulic diameter of the channel cross section defined as  $D_H = \frac{4A_C}{P_C} \cong 2H$ , where  $A_C$  and  $P_C$  are area and wetted perimeter of cylinders cross section.

In Eq. (6), subscript 0 denotes the values of plain channel with no cylinder and the tilde mark is the time average as follows:

$$\phi = \frac{1}{t_e - t_s} \int_{t_s}^{t_e} \phi \, dt \quad (9)$$

where  $\phi$  can be any of the parameters, e.g.  $Nu$ ,  $f$ ,  $C_f$  etc., and the over-bar is the space average as below:

$$\bar{\phi} = \frac{1}{x_e - x_s} \int_{x_s}^{x_e} \phi \, dt \quad (10)$$

Skin-friction coefficient is given as below:

$$C_f = \frac{2\tau_w}{\rho U_{in}^2} \quad (11)$$

where  $\tau_w$  is the total shear stress on the wall and is defined as:

$$\tau_w = \mu \left( \frac{\partial u^*}{\partial y^*} + \frac{\partial v^*}{\partial x^*} \right) \quad (12)$$

Moreover, drag coefficient for cylinders is

$$C_D = \frac{2F_D}{\rho U_{in}^2 b} \quad (13)$$

where  $F_D$  is the drag force per unit length. Strouhal number is defined as:

$$St = \frac{\omega b}{U_{in}} \quad (14)$$

where  $\omega$  is the vortex shedding frequency (Hz).

#### 2.5. Geometry

Geometry of the channel and cylinders is depicted in Fig. 1. As it shows for the first model,  $x_s$ , the end of the cylinder, is the beginning of the heated part of the wall. The fully developed flow enters from the left side with Eq. (5) and exits the right side. Moreover, the blockage ratio is defined as  $\beta = b/H$ .

#### 2.6. Time stepping and grid independency

A combination of triangular and quadrilateral elements is used in internal region. Two layers of quadrilateral elements are applied at boundary layer, and the mesh is calibrated for fluid dynamics. The results of grid independency for equilateral triangular cylinder at  $Re=150$  and  $\beta=0.25$  and corresponding values for  $\overline{Nu}$  and  $f$  are presented in Table 1. Eventually, grid number 3 is used due to acceptable accordance with the results of Srikanth et al. [21] and De and Dalal [20].

Computational domain is comprised of 297259 triangular elements and 6338 quadrilateral elements, where 3353 of them are in boundary layer. The maximum and minimum element sizes are 0.0635b and 0.0039b, respectively. Also, a dimensionless time step of 0.003 is considered. It should be noted that in order to neglect the early effects of the flow before  $t_s$ , limits of the time integral in Eq. (9) are considered to be  $t_s$  and  $t_e$ . As a result,  $t_s$  is the beginning of the vortex shedding, and  $t_e$  is assumed to be long enough, about  $(5 \times L) / U_{in}$ . Moreover,  $x_s$  and  $x_e$ , limits of the space integral in Eq. (10), are 1.5 and 7.5 for  $Nu$  and 0 and 10 for  $C_f$ .

### 3. Results and discussion

#### 3.1. Validation

The present paper is validated by works of Srikanth et al. [21] and De and Dalal [20]. Values of drag coefficient and Strouhal number for equilateral triangular cylinder for  $\beta=0.25$  are presented in Table 2. The results show, for instance at  $Re=150$ , 0.08% and 0.5% differences for drag coefficient and Strouhal number with the values of Srikanth et al. [21] and 1.2% and 2.2% differences with the values of De and Dalal [20], respectively. Therefore, the differences are considered acceptable and this simulation is considered to be valid.

#### 3.2. Flow analyzing

First of all, effects of variation in blockage ratio and Reynolds number on flow over the equilateral triangular cylinder is investigated. Variation of drag coefficient with blockage ratio is presented in Fig. 2. The trend shows that drag coefficient increases with an increase in blockage ratio. The drag is the force exerted by the fluid on the body in the direction of the flow. This force consists of two components: friction drag and pressure drag. The friction drag is applied by the shear stress on the surface of the body while the pressure drag stems from the pressure difference between the fore and aft of the body. Since the drag coefficient ( $C_D$ ) is independent of size of the obstacle and includes both pressure and friction drag, this rise with the blockage ratio can be interpreted by the growth of the wake region since the frictional component of the drag is constant for different sizes.

Fig. 3 shows this phenomenon clearly. These results are reported by De and Dalal [20] for triangular cylinder with  $1/12 \leq \beta \leq 1/3$  as well. In contrast, the growing of the drag coefficient with an increase in the Reynolds number is diminutive. Although this rise from an increase in Reynolds number reinforces the generation of the wake region, which augments the drag coefficient; it expands the growth of the boundary layer on the surface of the cylinder.

Growth in thickness of the boundary layer reduces the velocity gradient perpendicular to the surface of the body and reduces the friction drag. Furthermore, damping effects of the wall proximity at  $\beta=0.35$  attenuates the generation of the wake. Davis et al. [30] reported this increase of drag coefficient with the Reynolds number for a square cylinder; and De and Dalal [20] reported it for a triangular cylinder as well.

Fig. 4 shows skin-friction coefficient as a function of the blockage ratio and Reynolds number. With an increase in the blockage ratio and approaching the cylinder to the channel wall, the velocity gradient increases in the region between the wall and the cylinder. This phenomenon is the major contributor in increasing the mean skin-friction coefficient with blockage ratio (Fig. 5). Moreover, it is observed that an increase in Reynolds number decreases the skin-friction coefficient. This means that the rise in velocity is dominant against the velocity gradient in Eq. (11).

One of the major characteristics of flow around bluff bodies is the Strouhal number which denotes the frequency of the vortex shedding upon inertia force. To put it simply, Strouhal number is a measurement of the possibility and strength of vortex shedding.

Before flow begins to fluctuate, a pair of fixed vortices first appears in the wake of the cylinder. When Reynolds number reaches to its critical value, these vortices, which by now have stretched and elongated, become unstable and the first periodic driving forces begin. The subsequent behavior of this vorticity strongly influences the flow development and the forces acting on the body. Particularly, these vortices have strong influence on mass and heat mixture. Vortex shedding frequency is equal to the period of the fluctuations of perpendicular velocity component. Variation of the Strouhal number with  $\beta$  and  $Re$  is presented in Fig. 6.

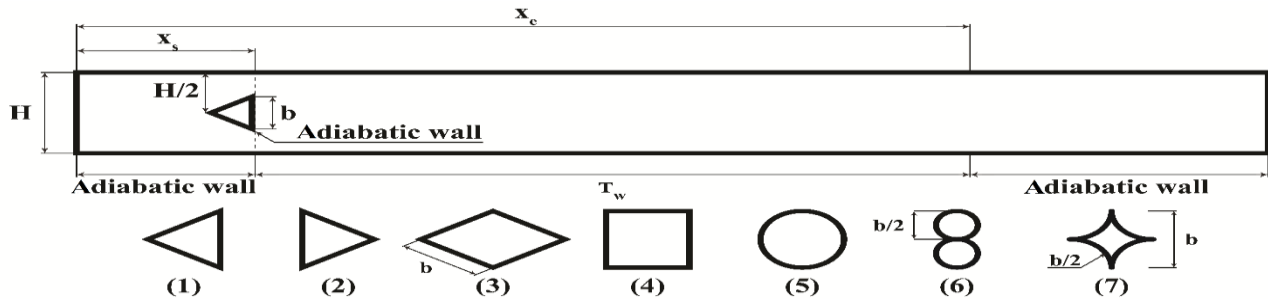


Fig. 1. Geometry of the problem.

Table 1. Grid independency for equilateral triangular cylinder at  $Re=150$  and  $\beta=0.25$ .

Grid number	Total triangular elements	Total quadrilateral elements	Boundary elements	$Nu$	$f$
G1	49097	3282	1731	6.3633	0.16229
G2	115311	6338	3309	6.4306	0.16772
G3	297259	6338	3353	6.5240	0.17495

Table 2. Validation by Srikanth et al. [21] and De and Dalal [20] for equilateral triangular cylinder for  $\beta=0.25$ .

Source	$C_D$	$St$
Re=80		
Present paper	1.6503	0.1900
Srikanth et al. [21]	1.6357	0.1919
De and Dalal [20]	1.64	0.195
Re=100		
Present paper	1.6817	0.2000
Srikanth et al. [21]	1.6708	0.2004
De and Dalal [20]	1.68	0.205
Re=150		
Present paper	1.9364	0.2200
Srikanth et al. [21]	1.9349	0.2212
De and Dalal [20]	1.96	0.225

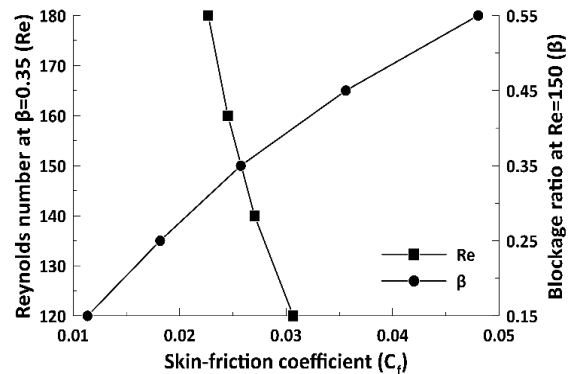


Fig. 4. Variation of the  $C_f$  with the Reynolds number at  $\beta=0.35$  and blockage ratio at  $Re=150$  for triangular cylinder.

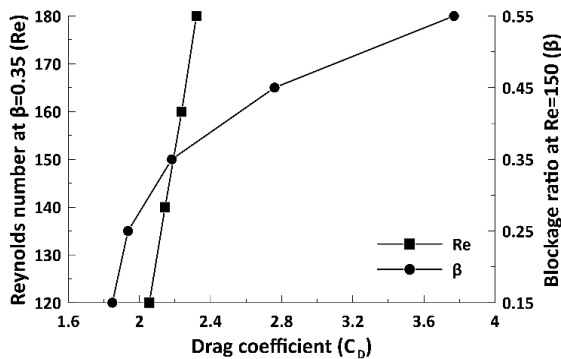


Fig. 2. Variation of the drag coefficient with the Reynolds number at  $\beta=0.35$  and blockage ratio at  $Re=150$  for triangular cylinder.

It reveals that at high blockage ratios effects of side walls are noteworthy, which make the frequency of the vortex shedding shift to higher values. This is in agreement with the results of De and Dalal [20] for the triangular cylinder at  $1/12 \leq \beta \leq 1/3$ , and Patil et al. [31] for the square cylinder at  $0.2 \leq \beta \leq 0.5$ . Also, an increase in Reynolds number for constant blockage ratio increases the Strouhal number, but not as much as the blockage ratio. An increase in Strouhal number with Reynolds number is reported by Srikanth et al. [21] and De and Dalal [20] for the triangular cylinder, Sharma and Eswaran [16] for the square cylinder and Norberg [32] for the circular cylinder.

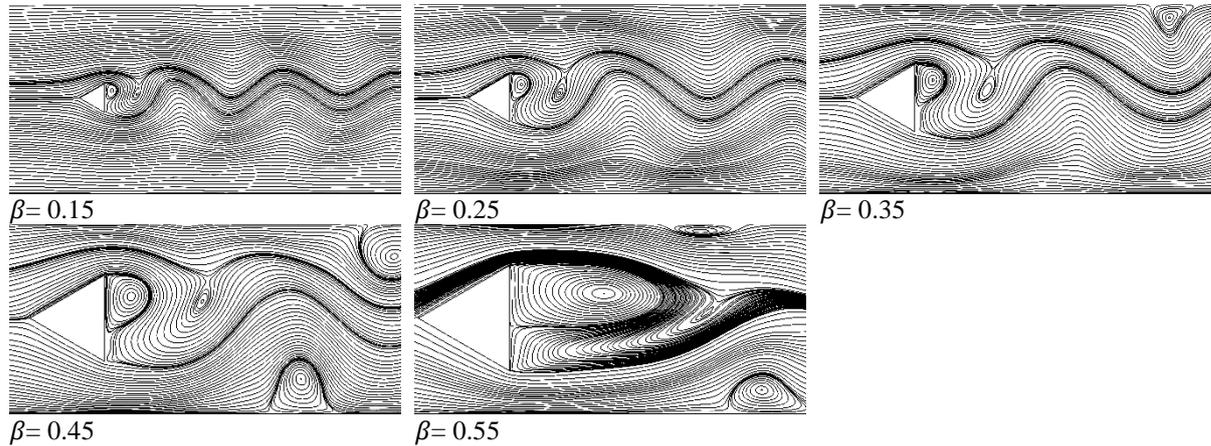


Fig. 3. Streamlines for blockage ratios between 0.15 and 0.55 at Re=15.

Fig. 7 demonstrates the variation of the pumping factor with the blockage ratio and Reynolds number. Pumping factor is a measurement of all dissipations in flow field, including wall friction and drag force.

This coefficient, particularly, is used in calculation of the Performance Index (PI) factor. As expected, with an increase in the blockage ratio, the pumping factor increases significantly as a result of rise in both drag and skin-friction coefficient; but with an increase in Reynolds number, pumping factor decreases slightly. This means that the decrease in the skin-friction dominates the increase of drag coefficient.

After investigating the effects of variation in Reynolds number and blockage ratio on flow characteristics, at this point, attention is turned toward variation in the shape of the cylinder. This part of the investigation is conducted to enhance the heat transfer efficiency (PI factor). As in Eq. (6), the PI factor is composed of Nusselt number and pumping factor.

Nusselt number will be discussed in subsection 3.3. Effects of modifying the shape of the cylinder on pumping factor will be discussed here. Additionally, to give more information and better illustration of flow around different cylinders, other coefficients are presented as well. In order to compare the impacts of different shapes of the cylinder, Reynolds number and blockage ratio are, respectively, assumed to be 180 and 0.35. At these values, fluctuation of the flow has the highest effect on the walls of the channel while damping effect of the walls on generation of the vortex shedding is the lowest. Comparing Figs. 8, 9, and 11 confirms that fore and aft pressure

difference, also, is responsible for an increase in skin-friction coefficient.

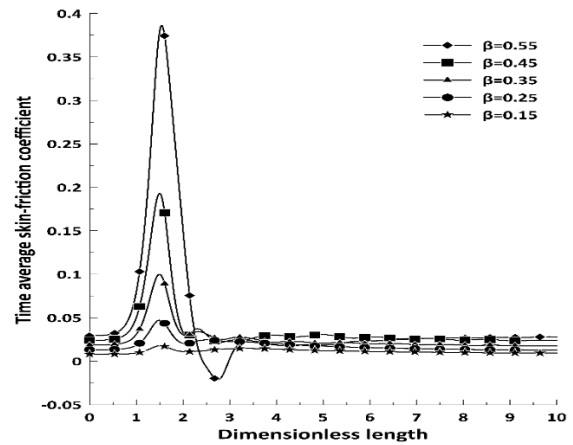


Fig. 5. Variation of the time average skin-friction coefficient with dimensionless length for different blockage ratios for triangular cylinder at Re=150.

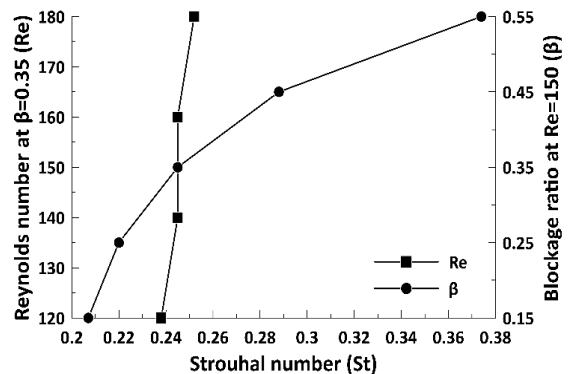


Fig. 6. Variation of Strouhal number with the Reynolds number at  $\beta=0.35$  and blockage ratio at Re=150 for triangular cylinder.

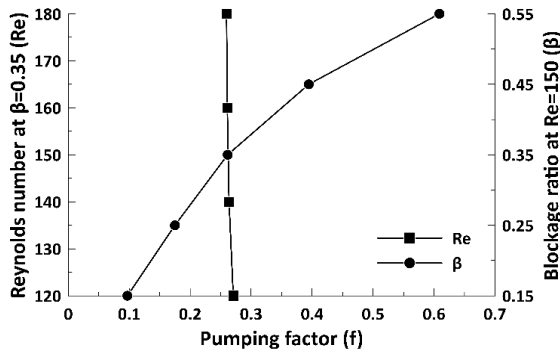


Fig. 7. Variation of the pumping factor with the Reynolds number at  $\beta=0.35$  and blockage ratio at  $Re=150$  for triangular cylinder.

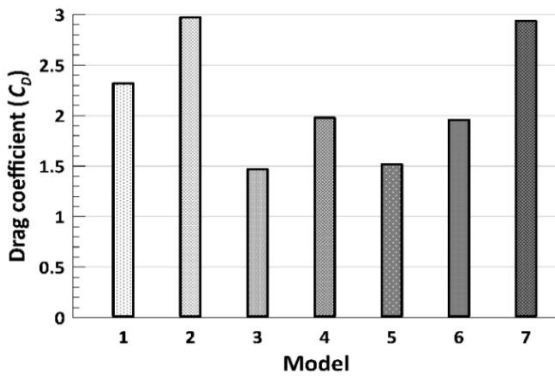


Fig. 8. Values of the drag coefficient for different shapes of the cylinder at  $Re=180$  and  $\beta=0.35$ .

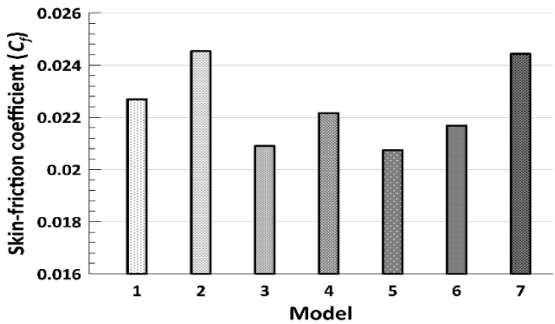


Fig. 9. Values of the skin-friction coefficient for different shapes of the cylinder at  $Re=180$  and  $\beta=0.35$ .

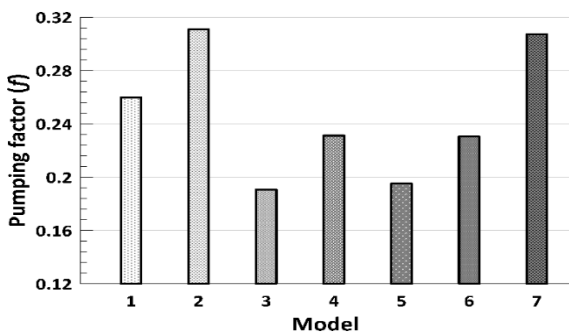


Fig. 10. Values of the pumping factor for different shapes of the cylinder at  $Re=180$  and  $\beta=0$ .

As the pressure difference increases, flow becomes more turbulent and velocity gradient rises near the wall. This leads to higher shear stress and skin-friction coefficient. Furthermore, the pumping factor, which can be explained as total effects of the drag force and shear stress, follows the same pattern in different shapes.

Figs. 11 and 12 present values of Strouhal number and streamlines for different shapes of the cylinder, respectively. Streamlines represent vortices that have a direct effect on the Stockholm number. Generally, Strouhal number depends on Reynolds number, the shape of the body, and the blockage ratio. Continuous shapes have no fixed dissection point. Therefore, it is more dependent on the Reynolds number; but in discontinuous shapes, the type and position of the vertices are important. For models 2 and 7, which have the highest values of the  $C_D$ ,  $C_f$ , and  $f$ , it is observed that the Strouhal number has the minimum values. On the other hand, it has the maximum value in model 4. Similarities in structure and geometry of the vortex shedding from different shapes drew attention of the scientists to the relationship between Strouhal number and size of the wake; Ahlborn et al.[33] and Balachandar et al. [34], for instance, made some effort on this aspect.

### 3.3. Heat transfer analyzing

Variation of the Nusselt number, which is a measurement of the heat transfer from side walls of the channel, versus Reynolds number and blockage ratio for equilateral triangular cylinder is presented in Fig. 13. As this figure demonstrates, an increase in Reynolds number augments vortex shedding and induces turbulent effects. Subsequently, this fluctuation improves mixing of the cold and hot fluid. In contrast, with an increase in blockage ratio, Nusselt number reaches to an optimum value at  $\beta=0.35$ . By more increase in blockage ratio, Nusselt number, as a result of damping effect of the walls on generation of the vortex shedding, declines and by then plummets down at  $\beta=0.55$ . However, at low blockage ratios ( $\beta=0.15$ ), it is observed that Nusselt number is higher. This is caused by the high inlet velocity. As mentioned earlier, at this blockage ratio the effect of the fluctuation of flow on side walls is trivial. More precisely, Fig. 14 clarifies the distribution of the Nusselt number for different blockage ratios. The impact of vortex shedding on heat transfer enhancement and decrease in heat transfer due to destruction of the vortex shedding is clearly shown in this figure and Fig. 15.

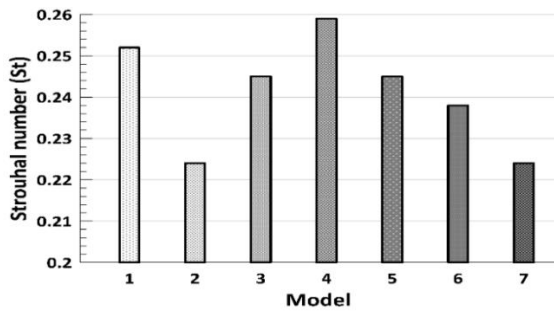


Fig. 11. Values of the Strouhal number for different shapes of the cylinder at  $Re=180$  and  $\beta=0.35$ .

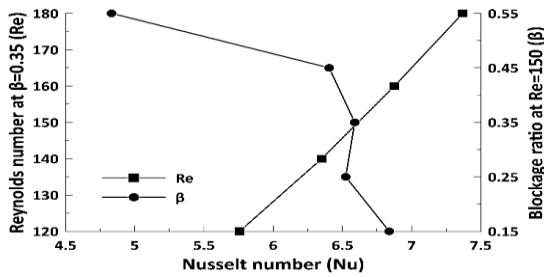


Fig. 13. Variation of Nusselt number with blockage ratio at  $Re=150$  and Reynolds number at  $\beta=0.35$  for triangular cylinder.

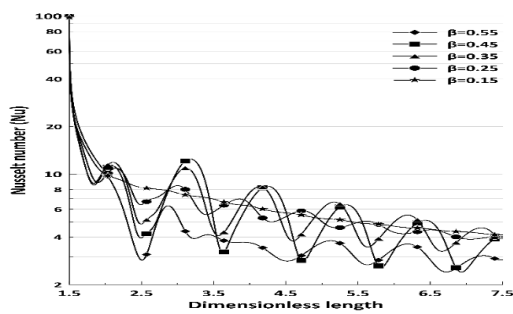


Fig. 14. Distribution of the Nusselt number for triangular cylinder for different blockage ratios at  $Re=150$ .

Fig. 16 presents values of the Nusselt number for different shapes of the built-in cylinder at  $Re=180$  and  $\beta=0.35$ . This figure reveals that model number seven and two have the highest values of the Nusselt number, respectively. By comparing Fig. 16 with Figs. 8, 9, and 10, it can be inferred that, generally, for models with stronger wake region, Nusselt number is higher. The reason is that by increasing the pressure difference between fore and aft of the cylinder, more fluid with higher velocity flows toward back of the cylinder. This phenomenon makes the flow more turbulent, which induces higher values of the Nusselt number. Perturbation of the thermal boundary layer for each cylinder is depicted in Fig. 17.

### 3.4. Thermal efficiency

The PI factor defines thermal efficiency of a channel in heat transfer enhancement with regard to the pumping factor. Fig. 18 shows PI factor as a function of blockage ratio and Reynolds number for the equilateral triangular cylinder (model one). As can be seen, with an increase in the Reynolds number the PI factor slightly decreases. Moreover, for different blockage ratios, the PI factor has an optimum range between  $\beta=0.35$  and  $\beta=0.45$ .

Fig. 19 presents the values of the PI factor for different shapes of the cylinder at  $Re=180$  and  $\beta=0.35$ . As this figure shows, the best cylinder shape from the thermal efficiency view point is model seven with  $PI=0.9736$ .

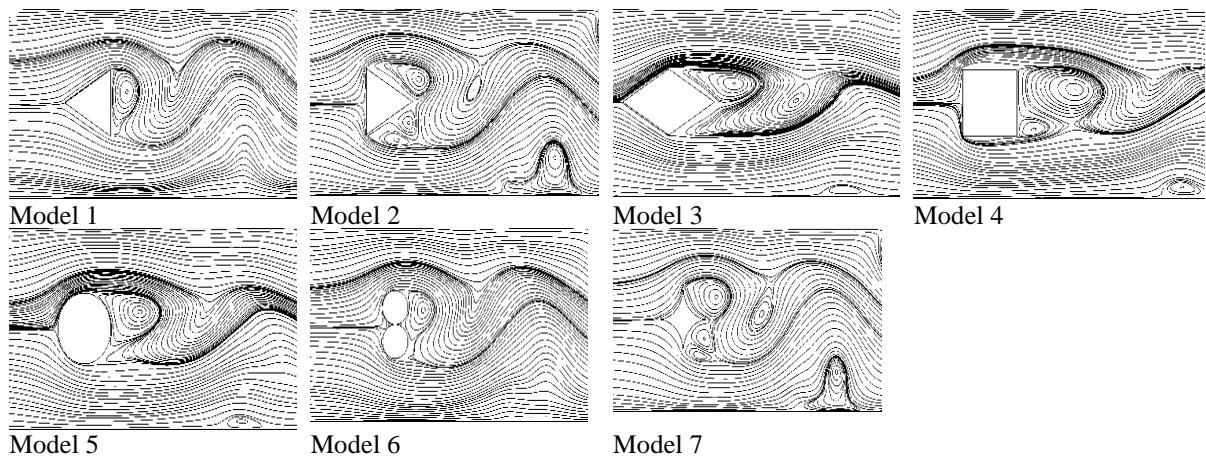


Fig. 12. Streamlines for different shapes of the cylinder at  $Re=180$  and  $\beta=0.3$ .

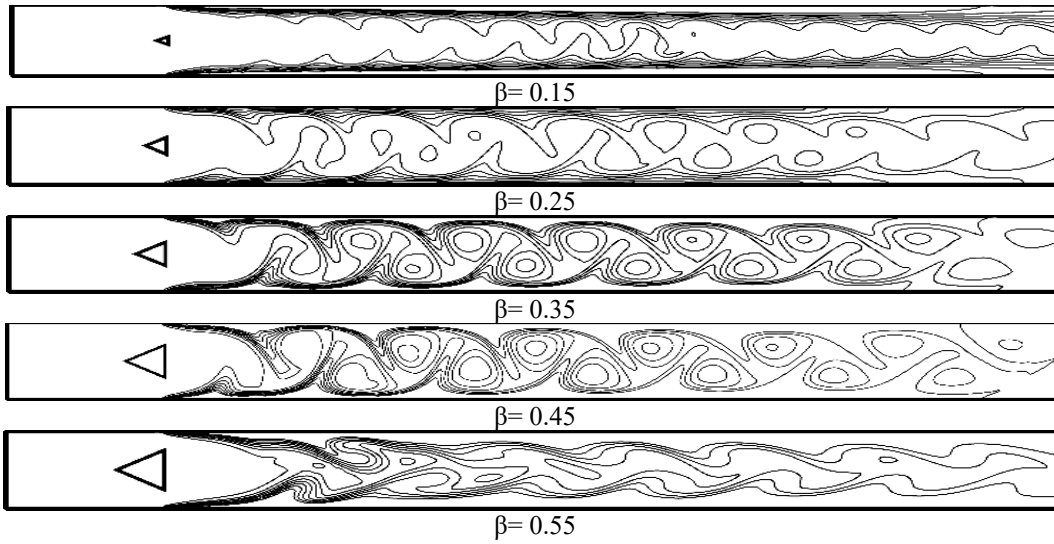


Fig. 15. Isothermal contours for different blockage ratios of the equilateral triangular cylinder at  $Re=150$ .

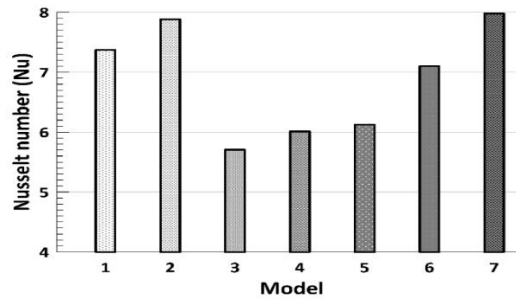


Fig. 16. Values of the Nusselt number for different shapes of the cylinder at  $Re=180$  and  $\beta=0.35$ .

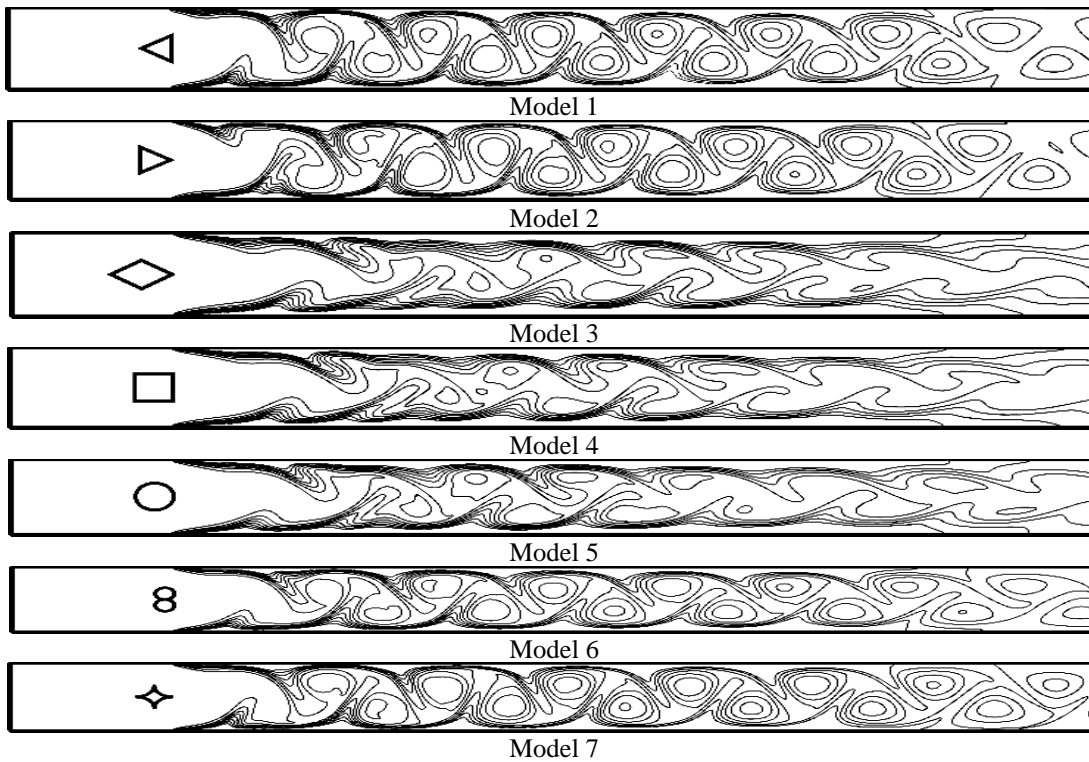


Fig. 17. Isothermal contours for different shapes of the cylinder at  $Re=180$  and  $B=0.35$ .

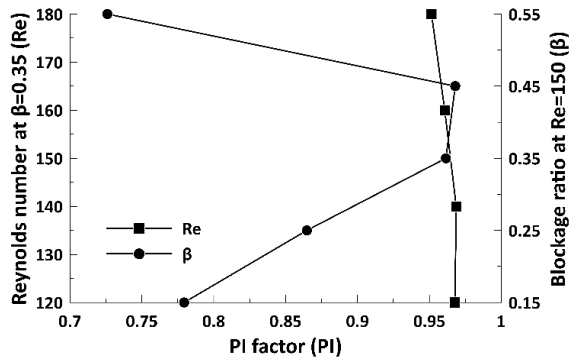


Fig. 18. Variation of the PI factor with the Reynolds number at  $\beta=0.35$  and blockage ratio at  $Re=150$  for triangular cylinder.

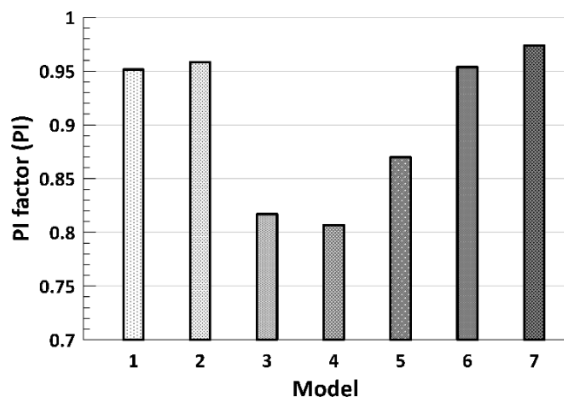


Fig. 19. Values of the PI factor for different shapes of the cylinder at  $Re=180$  and  $B=0.35$ .

#### 4. Conclusions

The present study is conducted to investigate 2-D laminar air flow and heat transfer characteristics of a channel with a built-in cylinder. Variation of the cylinder’s drag coefficient, Strouhal number, skin-friction factor, pumping factor, Nusselt number from side walls of the channel, and PI factor for  $120 \leq Re \leq 180$  and  $0.15 \leq \beta \leq 0.55$  is studied for the equilateral triangular cylinder. Results show that for the constant blockage ratio of 0.35, the drag coefficient, Nusselt number, and Strouhal number increase, but the skin-friction coefficient, pumping factor, and PI factor decrease with an increase in Reynolds number.

Also, with increase in blockage ratio at constant Reynolds number,  $Re=150$ , the drag coefficient, skin-friction coefficient, Strouhal number, and pumping factor increase, but the Nusselt number decreases and the PI factor shows an optimum range for  $0.35 \leq \beta \leq 0.45$ . Moreover, it is seen that

variation in the blockage ratio has more significant effects on flow characteristics. For  $\beta > 0.45$  fluctuation of flow is destroyed by damping effects of the side walls. In the second orientation, variation in the shape of the built-in cylinders is investigated for seven different types of geometry. Findings prove that values of the drag coefficient, skin-friction coefficient, pumping factor, and Nusselt number are higher for the second and seventh models. Furthermore, results show a direct correlation between the drag coefficient, skin-friction coefficient, pumping factor, and Nusselt number. Finally, the maximum accessible PI factor of 0.9736 is obtained for the seventh model.

#### References

- [1] L. Wang, M. M. Alam and Y. Zhou, “Two tandem cylinders of different diameters in cross-flow: Effect of an upstream cylinder on wake dynamics”, *J. Fluid Mech.*, Vol. 836, pp. 5-42, (2018).
- [2] F. Zafar and M. M. Alam, “A low Reynolds number flow and heat transfer topology of a cylinder in a wake”, *Phys. Fluids*, Vol. 30, No. 8, pp. 083603, (2018).
- [3] S. Yagmur, S. Dogan, M. H. Aksoy, E. Canli and M. Ozgoren, “Experimental and numerical investigation of flow structures around cylindrical bluff bodies”, *In EPJ Web of Conferences*, Vol. 92, pp. 02113, (2015).
- [4] J. Taghinia, M. M. Rahman, and T. Siikonen, “Large eddy simulation of flow past a circular cylinder with a novel sub-grid scale model”, *Eur. J. Mech. B Fluids*, Vol. 52, pp. 11-18, (2015).
- [5] R. M. Stringer, J. Zang, and A. J. Hillis, “Unsteady RANS computations of flow around a circular cylinder for a wide range of Reynolds numbers”, *Ocean Eng.*, Vol. 87, pp. 1-9, (2014).
- [6] W. Zhong, S. C. Yim and L. Deng, “Vortex shedding patterns past a rectangular cylinder near a free surface”, *Ocean Eng.*, Vol. 200, pp.107049, (2020).
- [7] K. S. Arjun and R. Kumar, “Performance Index in MHD Duct Nanofluid Flow Past a Bluff Body at High  $Re$ ”, *Stroj. Vestn-J Mech. E.*, Vol. 63, No. 4, (2017).

- [8] R. D. Selvakumar and S. Dhinakaran, "Forced convective heat transfer of nanofluids around a circular bluff body with the effects of slip velocity using a multi-phase mixture model", *Int. J. Heat Mass Transf.*, Vol. 106, pp. 816-828, (2017).
- [9] K. S. Arjun and K. Rakesh, "Heat transfer in magnetohydrodynamic nanofluid flow past a circular cylinder", *Phys. Fluids*, Vol. 32, No. 4, p. 045112, (2020).
- [10] D. H. Yoon, K. S. Yang and C. B. Choi, "Flow past a square cylinder with an angle of incidence", *Phys. Fluids*, Vol. 22, No. 4, pp. 043603, (2010).
- [11] T. Johnson and P. Joubert, "The influence of vortex generators on the drag and heat transfer from a circular cylinder normal to an airstream", *J Heat Trans-TASME*, Vol. 91, No. 1, pp. 91-99, (1969).
- [12] B. R. Noack and H. Eckelmann, "A low-dimensional Galerkin method for the three-dimensional flow around a circular cylinder", *Phys. Fluids*, Vol. 6, No. 1, pp. 124-143, (1994).
- [13] M. Zdravkovich, "Different modes of vortex shedding: an overview", *J. Fluid Struct.*, Vol. 10, No. 5, pp. 427-437, (1996).
- [14] C. H. Williamson, "Vortex dynamics in the cylinder wake", *Annu. Rev. Fluid Mech.*, Vol. 28, No. 1, pp. 477-539, (1996).
- [15] H. Suzuki, Y. Inoue, T. Nishimura, K. Fukutani and K. Suzuki, "Unsteady flow in a channel obstructed by a square rod (criss-cross motion of vortex)", *Int J Heat Fluid Flow*, Vol. 14, No. 1, pp. 2-9, (1993).
- [16] A. Sharma and V. Eswaran, "Effect of channel confinement on the two-dimensional laminar flow and heat transfer across a square cylinder", *Numer. Heat Transfer Part A.*, Vol. 47, No. 1, pp. 79-107, (2004).
- [17] A. Sharma and V. Eswaran, "Heat and fluid flow across a square cylinder in the two-dimensional laminar flow regime", *Numer. Heat Transfer part A.*, Vol. 45, No. 3, pp. 247-269, (2004).
- [18] K. Tatsutani, R. Devarakonda and J. Humphrey, "Unsteady flow and heat transfer for cylinder pairs in a channel", *Int. J. Heat Mass Transfer*, Vol. 36, No. 13, pp. 3311-3328, (1993).
- [19] A. Valencia, "Numerical study of self-sustained oscillatory flows and heat transfer in channels with a tandem of transverse vortex generators", *Heat Mass Transfer*, Vol. 33, No. 5-6, pp. 465-470, (1998).
- [20] A. K. De and A. Dalal, "Numerical study of laminar forced convection fluid flow and heat transfer from a triangular cylinder placed in a channel", *J. Heat Transfer-T ASME*, Vol. 129, No. 5, pp. 646-656, (2007).
- [21] S. Srikanth, A. Dhiman and S. Bijjam, "Confined flow and heat transfer across a triangular cylinder in a channel", *Int. J. Therm. Sci.*, Vol. 49, No. 11, pp. 2191-2200, (2010).
- [22] M. Ali, O. Zeitoun, and A. Nuhait, "Forced convection heat transfer over horizontal triangular cylinder in cross flow", *Int. J. Therm. Sci.*, Vol. 50, No. 1, pp. 106-114, (2011).
- [23] M. Farhadi, K. Sedighi and A. M. Korayem, "Effect of wall proximity on forced convection in a plane channel with a built-in triangular cylinder", *Int. J. Therm. Sci.*, Vol. 49, No. 6, pp. 1010-1018, (2010).
- [24] N. Agrwal, S. Dutta and B. K. Gandhi, "Experimental investigation of flow field behind triangular prisms at intermediate Reynolds number with different apex angles", *Exp. Therm. Fluid Sci.*, Vol. 72, pp. 97-111, (2016).
- [25] Y. Bao, D. Zhou and Y. J. Zhao, "A two-step Taylor-characteristic-based Galerkin method for incompressible flows and its application to flow over triangular cylinder with different incidence angles", *Int. J. Numer. Methods Fluids*, Vol. 62, No. 11, pp. 1181-1208, (2010).
- [26] J. Tu, D. Zhou, Y. Bao, Z. Han and R. Li, "Flow characteristics and flow-induced forces of a stationary and rotating triangular cylinder with different incidence angles at low Reynolds numbers", *J. Fluid Struct.*, Vol. 45, pp. 107-123, (2014).
- [27] D. Chatterjee and B. Mondal, "Mixed convection heat transfer from an equilateral triangular cylinder in cross flow at low Reynolds numbers", *Heat Transfer Eng.*, Vol. 36, No. 1, pp. 123-133, (2015).

- [28] A. Dhiman and R. Shyam, "Unsteady heat transfer from an equilateral triangular cylinder in the unconfined flow regime", *ISRN Mech. Eng.*, Vol. 2011, pp. 13, (2011).
- [29] D. Chatterjee and B. Mondal, "Forced convection heat transfer from an equilateral triangular cylinder at low Reynolds numbers", *Heat Mass Transfer*, Vol. 48, No. 9, pp. 1575-1587, (2012).
- [30] R. Davis, E. Moore and L. Purtell, "A numerical-experimental study of confined flow around rectangular cylinders", *Phys. Fluids*, Vol. 27, No. 1, pp. 46-59, (1984).
- [31] P. P. Patil and S. Tiwari, "Effect of blockage ratio on wake transition for flow past square cylinder", *Fluid Dyn. Res.*, Vol. 40, No. 11-12, pp. 753, (2008).
- [32] C. Norberg, "Flow around a circular cylinder: aspects of fluctuating lift", *J Fluid Struct.*, Vol. 15, No. 3-4, pp. 459-469, (2001).
- [33] B. Ahlborn, M. L. Seto and B. R. Noack, "On drag, Strouhal number and vortex-street structure", *Fluid Dyn. Res.*, Vol. 30, No. 1, pp. 379, (2002).
- [34] S. Balachandar, R. Mittal and F. Najjar, "Properties of the mean recirculation region in the wakes of two-dimensional bluff bodies", *J. Fluid Mech.*, Vol. 351, pp. 167-199, (1997).

Copyrights ©2021 The author(s). This is an open access article distributed under the terms of the Creative Commons Attribution (CC BY 4.0), which permits unrestricted use, distribution, and reproduction in any medium, as long as the original authors and source are cited. No permission is required from the authors or the publishers.



### How to cite this paper:

Sajad Rezazadeh, Mohammadreza Mataji Amirrud, Mohammad Raad and Davoud Abbasinezhad Fallah, "Numerical study of built-in cylinders' effects on flow pattern and heat transfer characteristics in a laminar channel flow," *J. Comput. Appl. Res. Mech. Eng.*, Vol. 11, No. 1, pp. 177-189, (2021).

**DOI:** 10.22061/JCARME.2020.6839.1880

**URL:** [https://jcarme.sru.ac.ir/?\\_action=showPDF&article=1495](https://jcarme.sru.ac.ir/?_action=showPDF&article=1495)

